"High-Resolution, Ultra-Sensitive Magnetic Imaging Using an Ensemble of Nitrogen-Vacancy (NV) Centers in Diamond"

July 26, 2013

Sponsored by

Defense Advanced Research Projects Agency (DOD)
(Controlling DARPA Technical Office)

ARPA Order I642-00

Issued by U.S. Army Contracting Command – Redstone
Under
Contract No. W31P4Q-13-C-0064

Name of Contractor:	Quantum Diamond Technologies Inc.
Principal Investigator, Project Scientist, or Engineer:	Colin Connolly
Business Address:	4 Brattle Street, Suite 209, Cambridge, MA 02138
Phone Number:	(617) 320-4105

Effective Date of Contract:	November 30, 2012
Short Title of Work:	Final Technical Report
Contract Expiration Date:	September 3, 2013
Reporting Period:	November 30 – July 26, 2013

DISCLAIMER

Table of Contents

Introduction

Overview

Imaging of weak magnetic fields at ambient temperatures and pressures with submicron spatial resolution and wide field of view is an outstanding challenge of great importance in both the physical and life sciences. A robust instrument able to image such magnetic fields will have wide-ranging and far-reaching applications in science and technology, including: minimally-invasive imaging of functional activity and magnetic structures in living cells; imaging and detection of magnetically-labeled cells and sub-cellular structures; non-destructive imaging of integrated circuits and stress in metallic joints; and probing magnetic order and domain structure in low-dimensional systems such as graphene, anti-ferromagnetic and multiferroic materials. To enable development in these areas, there is a need for a general-purpose instrument platform for magnetic field imaging with diamond.

Quantum Diamond Technologies Inc. (QDTI) made significant progress in Phase I of this SBIR effort toward developing such a platform. Additionally, QDTI demonstrated the feasibility for a powerful new application of diamond magnetic imaging: rapid detection of rare biological targets in blood and other biofluids. One target in particular, circulating tumor cells (CTCs) in the bloodstream, has been clinically correlated with cancer progression. CTCs are thought to play an important role in seeding of metastatic tumor sites, a process that dramatically increases patient mortality. However, CTC diagnostic technology is lacking; existing tools are expensive, slow, insufficiently sensitive, and cumbersome for clinicians and researchers. Diamond magnetic imaging has the capability to excel where these tools fall short, by combining high-fidelity magnetic detection of magnetically-labeled cells with high-throughput, wide-field diamond magnetic imaging.

Magnetic sensing with diamond

Members of the QDTI team at Harvard University first proposed and experimentally demonstrated magnetometry using nitrogen-vacancy (NV) color centers in diamond [1, 2], showing that a single NV center at room temperature can provide magnetic field sensitivity below 10 $nT/Hz^{1/2}$. In the past several years, many magnetometer modalities have been developed at Harvard [3–10] and elsewhere [11–16], and the unique capabilities of diamond magnetometry have been employed to answer outstanding scientific questions.

The NV color center is a localized defect in diamond formed by a nitrogen atom in place of one carbon atom in the diamond crystal lattice, combined with a vacancy in one of the four neighboring sites. The nitrogen and vacancy lattice sites define the axis of the NV electronic spin, which is $S = 1$ for the negatively charged NV^- center (the focus of this report). The NV electronic ground state consists of three spin sublevels, $m_S = 0$ and ± 1. In the absence of external fields, the $m_S = 0$ state is separated from $m_S = \pm 1$ by a 2.87-GHz zero-field splitting. The large electronic Zeeman interaction with external magnetic fields splits the $m_S = \pm 1$ sublevels, allowing spectral isolation of a single electronic spin transition for high-precision magnetometry [1, 2].

The NV center in diamond stands out among solid-state systems because the NV electronic spin state can be efficiently prepared, manipulated, and measured with optical and microwave excitation at room temperature while maintaining long-lived spin coherence lifetimes ($T_2 > 1$ ms for high-purity diamond). Illumination with green laser light polarizes the NV ground state into the $m_S = 0$ state due to non-radiative, non-spin-preserving transitions through metastable electronic states. In addition, these spin-dependent transitions lead to a ground-state spin dependence of the intensity of red NV fluorescence, allowing for optical state detection. Once polarized, the NV electronic spin state can be manipulated

with microwave fields using standard electron spin resonance (ESR) techniques. In particular, appropriate ESR pulse sequences (e.g., Ramsey, Hahn-echo, multi-pulse CPMG and XY), together with NV spin-state-dependent red fluorescence, can provide high-sensitivity measurements of external magnetic fields [7, 17], including AC, DC and fluctuating (incoherent) fields.

The small size of the NV center allows for unprecedented magnetic sensitivity with nanoscale resolution. Many NV centers can be deterministically grown or implanted into diamond to provide a $N^{1/2}$ enhancement. Sensitivity of 100 pT/Hz$^{1/2}$ has been demonstrated [6], with much higher sensitivity expected soon with straightforward improvements. In addition, a large array of NV centers can be imaged with standard microscopy techniques to generate high-resolution wide-field images of magnetic fields at the diamond surface [3, 10].

Diamond sensors can achieve this capabilities at room temperature using a compact, robust, and biocompatible package without direct electrical contacts to the sensor. This is in contrast to other high-sensitivity magnetometry technologies based upon the Hall effect, optical rotation in alkali vapors, or superconductors (SQUIDs) at low temperatures. Furthermore, wide-field magnetic imaging enables millions of sub-micron magnetic field measurements to be made in parallel using a single millimeter-sized diamond sensor.

Improving cancer diagnostics and treatment through detection of blood-borne tumor cells

Over 1.6 million Americans will receive a diagnosis of cancer in 2013 and nearly 600,000 people will die from the disease [18], making it the leading cause of death in the United States after heart disease [19]. Cancer is most deadly when it infiltrates many points in the body through the metastasis, or spread, of cancer cells from a primary tumor to other organs, after which patient survival rates markedly drop [18]. Predicting metastasis, however, remains a significant clinical challenge. The chemical, physical and biological triggers and mechanisms of metastasis are a very active area of research that is beginning to bear fruit to guide development of improved diagnostic tests, disease prognosis, and targeted drug therapies.

One such vein of research has focused on CTCs in the bloodstream, which have received increased attention due to clinical studies demonstrating a strong correlation between elevated CTC levels and cancer progression [20]. The presence of cancer cells in the bloodstream fits well with the so-called "seed and soil" hypothesis of metastasis, in which such cells adhere in sites with favorable qualities for tumor cell growth, thus spreading the cancer. Furthermore, in some cases CTC concentration has also been observed to decrease in response to chemotherapy and remain low during periods of remission [21]. The utility of enumerating CTCs in patient blood is therefore clear: with only occasional blood draws, a clinician might gain insight into the patient's disease, her prognosis, and her response to treatment regimens. Such a diagnostic tool would be an invaluable asset to complement other diagnostic approaches, which can be invasive (such as surgical biopsy) and expensive (such as magnetic resonance imaging), and which may require ionizing radiation (such as computed X-ray tomography) that is itself carcinogenic.

CTC enumeration is made difficult, however, by the low concentrations at which CTCs are found. Amid billions of normal cells in 1 mL of blood there may be as few as one CTC. Therefore, CTC enumeration assays must be extremely sensitive to avoid undercounting the rare target cells, while also ensuring that the detection threshold does not produce false positives from the sea of normal candidate cells. Existing technologies in use for CTC enumeration (such as CellSearch by Veridex, the only FDA-approved platform) are expensive, slow, and lack the sensitivity necessary to harness the clinical utility of CTCs for improved treatment.

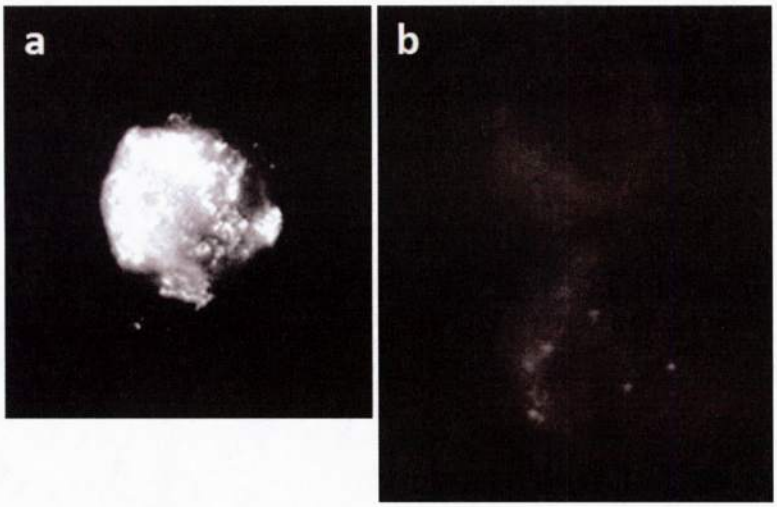

Figure 1: Optical microscopy of human breast cancer cells (SK-BR-3) illuminated with 410 ±40-nm light, observed through a 535 ±50-nm filter. The cell in (a) has been conjugated to particles containing FITC dye molecules, which fluoresce brightly with these excitation and collection bandwidths. In contrast, No fluorescent dye molecules are present in (b), but considerable levels of autofluorescence are still visible. Such unintended light causes false positive detections in fluorescence-based cell counting devices.

Rapid, accurate detection of CTCs with diamond

Magnetic detection is well suited to the challenge of detecting a few CTCs amid a large background of normal cells. CTCs can be specifically targeted and magnetically labeled using antibodies that bind only to certain markers that are numerous on cancerous cells. Magnetic signals from labeled cells can be detected with high sensitivity due to the intrinsically low background of magnetic noise in most biological samples. In contrast, optical fluorescence signals from fluorophores or quantum dots must compete with nonspecific fluorescence of the biological sample itself (autofluorescence), which is emitted from natural compounds such as metabolic proteins (Figure 1). In addition, the magnetic field from the cell permeates through other cells and contaminants to provide a reliable signal for detection, even from opaque samples. Hence superior fidelity can be obtained with magnetic detection [22], and with minimal sample processing or waste of target cells.

Diamond magnetic imaging adds to these advantages the capacity for rapid parallel detection, since many cells can be imaged at once over a wide field of view. A sensor surface of 1 cm^2 can accommodate roughly one million candidate cells in a monolayer (Figure 2) and can be imaged in parallel onto a many-

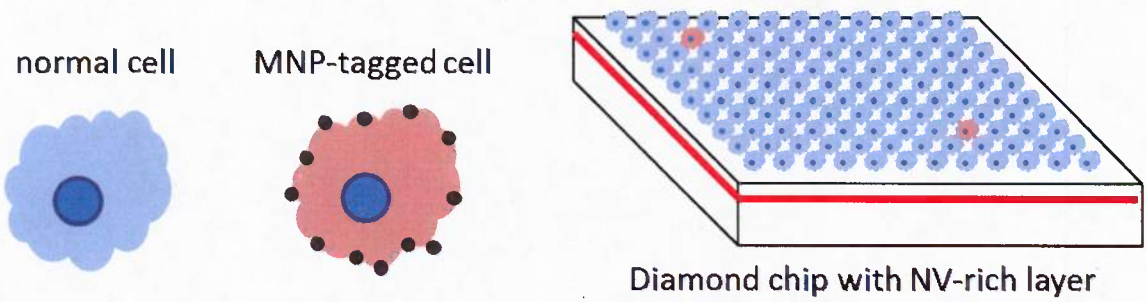

Figure 2: Schematic of the concept of a rare cell detection platform based upon a diamond NV magnetic sensor. A diamond plate is engineered to have a thin layer with a high density of NV centers. Candidate cells are introduced on the diamond surface and NV center fluorescence from the entire sensor is collected to determine the magnetic field below each cell. Cells labeled with magnetic nanoparticles (MNPs) stand out clearly with magnetic fields well above the low magnetic noise background.

megapixel CCD or CMOS array. Scanning the millions of nucleated cells present in a standard patient sample would therefore require only a few separate scans, which could be completed in well under an hour even if each took a full minute. Importantly, this assay need not affect the viability of the target cells, and is compatible with subsequent enrichment for further analysis, such as genetic identification of cancer type, or of concurrent use of optical fluorescent microscopy.

The combination of high-fidelity magnetic detection and wide-field diamond magnetic imaging presents a powerful new clinical and research tool. This technology has the capacity to address the serious drawbacks of existing tools for CTC enumeration, including cost, sensitivity and speed. Diamond magnetic imaging can provide a qualitatively better cancer diagnostic device for improving patient care, accelerating research development, and reducing the cost of treatment.

Phase I technical objectives

The objectives of QDTI's Phase I effort were twofold: (1) to identify a high-value target application for wide-field diamond magnetic imaging and demonstrate its feasibility; and (2) to develop techniques for improved diamond imager performance. These objectives were met, and the results are summarized here.

1. Identification of the target application

Phase I effort commenced with market research. QDTI assessed a number of potential commercial applications of magnetic field imaging with diamond. This included assessing the technological requirements for each and the specific competitive advantages (and disadvantages) of diamond sensing compared to the wide array of existing, mature magnetometer technologies. In particular, diamond sensors are set apart by their ability to sense magnetic fields in extreme conditions or in biological environments with sub-micron resolution over millions of simultaneous channels, which enables a number of novel magnetic sensing modalities.

QDTI identified a CTC detection assay as the focus application of Phase I. The assay uses wide-field magnetic imaging with a diamond sensor chip to detect cancer cells labeled with magnetic nanoparticles (MNPs). Magnetic labeling creates predictable magnetic field patterns that are many orders of magnitude stronger than the magnetic background in natural biological environments (for example, those backgrounds created by spin fluctuations in ionic solutions or by inhomogeneity of magnetic susceptibility within and between cells). Unlike the intrinsic autofluorescence which complicates optical detection of fluorescent labels such as dye molecules or quantum dots (Figure 1), the very low magnetic background enables cell detection with very high sensitivity and specificity.

Recent research has demonstrated that magnetic imaging provides superior detection fidelity and is more robust to sample contamination than gold standard optical detection methods [22]. QDTI determined that using diamond magnetic sensors could improve this technology further by allowing for rapid parallel detection of many cells simultaneously. Such an assay would address two critical goals of CTC detection which have not yet been simultaneously achieved: (1) highly accurate and sensitive detection of nearly all CTCs in a patient sample using a variety of cellular markers; and (2) total assay time well under an hour.

2. Magnetic imaging apparatus and procedure

A schematic of the magnetic imaging apparatus is shown in Figure 3. MNP-tagged cells are introduced to the surface of a 2 mm × 2 mm diamond chip, a region of which has a thin (about 7 nm thickness) layer of NV centers implanted about 20 nm below the surface at a density of about 3×10^{11} cm^{-2}. This NV

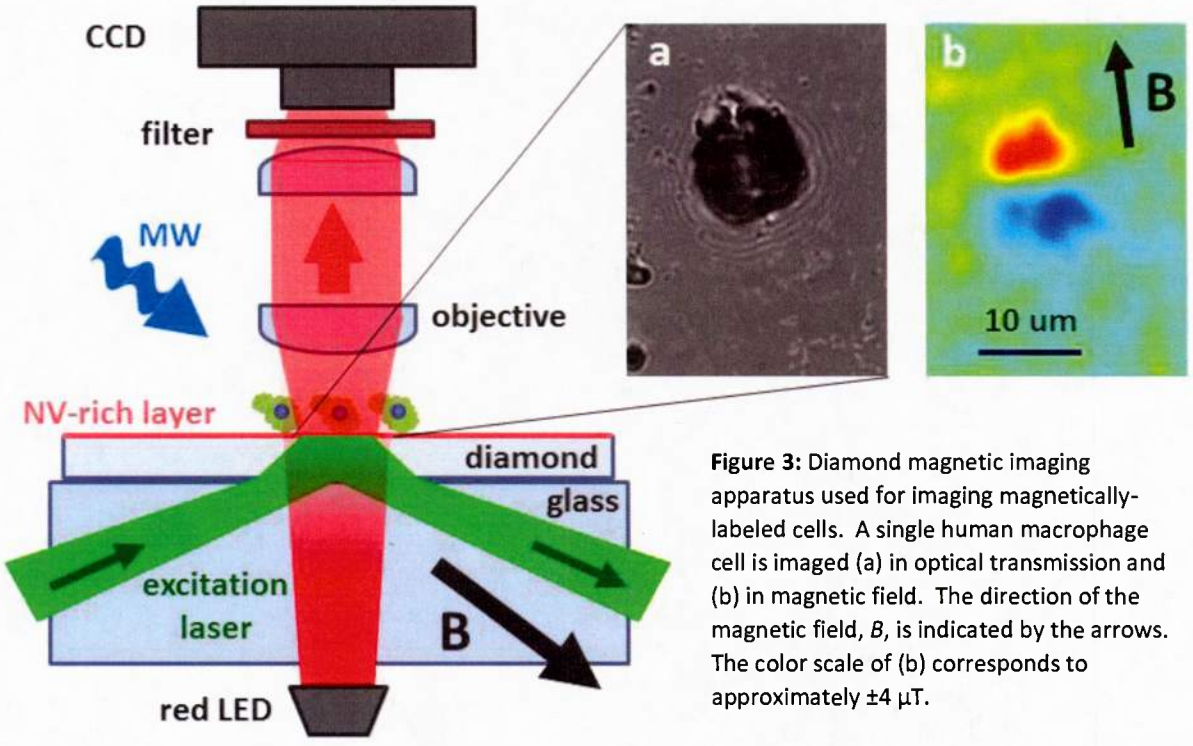

Figure 3: Diamond magnetic imaging apparatus used for imaging magnetically-labeled cells. A single human macrophage cell is imaged (a) in optical transmission and (b) in magnetic field. The direction of the magnetic field, *B*, is indicated by the arrows. The color scale of (b) corresponds to approximately ±4 μT.

layer is illuminated from below with a 532-nm excitation laser, which is totally internally reflected at the surface adjacent to the cells. Red fluorescence from the NV centers is collected by an objective lens and imaged onto a CCD camera through an optical filter that blocks scattered excitation light. Alternately, a red LED below the diamond can illuminate the cells for optical imaging. Microwaves near 3 GHz radiate from a simple wire loop to drive transitions between magnetic sublevels of the NV ground state, for electron spin resonance (ESR) measurements. Finally, a static magnetic bias field of about 24 mT is applied, aligned to one of the four diamond crystal axes, which includes components both normal and parallel to the diamond surface (the 100 crystal plane).

The MNPs used in Phase I are superparamagnetic iron oxide particles, with core diameters between 7 and 20 nm. Superparamagnetism refers to the case in which the time scale for magnetic relaxation of the MNP is much shorter than the measurement time, such that the MNP magnetization can be treated as always in equilibrium [23]. Under such conditions, the MNPs behave as strongly paramagnetic particles and their magnetic moments align rapidly with a modest external applied field, without hysteresis or significant zero-field magnetization. This is a powerful effect for generating much larger magnetic fields than would be achieved with a thermal polarization of non-interacting electron spins.

On the surface of each cell, all MNP tags are magnetized by the magnetic field to produce a cumulative dipole-like cellular field. To image this field, a series of camera exposures are taken under identical laser excitation while varying the microwave frequency across the Zeeman-shifted NV ESR resonance. The set of fluorescence images constitutes one ESR measurement for each pixel. Fitting separately at each pixel gives the resonance center location, which the cellular field shifts locally by approximately 28 kHz/μT. Hence the local magnetic field projection onto the NV axis is determined for all pixels. While all NV centers fluoresce under laser excitation, only one quarter of the NV centers contribute to the resonant ESR feature, since only these have their NV axis aligned with the magnetic field.

3. Feasibility studies for rare cell detection

To evaluate the use of diamond magnetic imaging for rare cell detection, QDTI performed a series of feasibility studies. This work was facilitated by collaborations formed with researchers who have specific expertise and interest in the target application: Prof. Hakho Lee of the Center for Systems Biology at Massachusetts General Hospital (MGH), who has invented novel methods of magnetic detection of MNP-tagged cells, including CTCs [22]; and Dr. Ron Walsworth of the Harvard-Smithsonian Center for Astrophysics, who has pioneered biological applications of wide-field magnetic imaging with diamond [10].

Cell labeling was performed in Phase I at MGH using two methods: (1) MNP internalization by mouse macrophages; and (2) surface labeling with antibodies of human breast cancer cells. In both cases (macrophages and cancer cells), the cells were fixed in formaldehyde after magnetic targeting, after which they remained stable for many days.

Macrophages are immune system cells that readily internalize foreign material from the extracellular fluid in a process called phagocytosis. When macrophages are incubated with MNPs, the cells become loaded with particles [24] without the need for additional conjugation steps. This makes macrophages an attractive test bed for early-stage testing. In QDTI's initial study, approximately 100 μL of a suspension of MNP-loaded mouse macrophages (RAW 264.7 cell line) was put in a small reservoir surrounding the diamond sensor and allowed to dry. Desiccated cells were located on the diamond surface using optical transmission microscopy, and the corresponding field of view was magnetically imaged (Figure 3). Due to the MNPs trapped within the cell, a dipole-like magnetic field distortion of approximately ±4 μT is clearly visible, oriented in the direction of the bias magnetic field.

To be useful for rare cell detection, however, it is critical that magnetic imaging be more broadly applicable for detecting specific populations of target cells. Hence, subsequent work extended detection to cells labeled using the second method: immunological labeling with antibodies. MNPs were attached to breast cancer cells (SK-BR-3 cell line) using antibodies that bind to the Her2 surface marker (antigen). The antibodies bind exclusively to this marker, allowing for up to a million MNPs to be attached to the surface of each cell [22]. The antibodies were, in turn, conjugated to biotin, which binds tightly to a coating of streptavidin covalently bonded to the MNP surface. Figure 4 shows optical and magnetic imaging of magnetically-labeled cancer cells, with each producing a distinct dipole distortion.

With these feasibility studies, QDTI demonstrated the potential for detection of magnetically-labeled cells using diamond magnetic imaging. The high signal to noise ratio (SNR) further suggests that such signals will stand out clearly above background noise, allowing for a small minority fraction of target cells to be identified from other candidates. Following this success, the remainder of the Phase I effort was devoted to improving the technical performance of the diamond magnetic imager and making further progress toward a diamond-based rare cell detector.

4. Technical progress: magnetic imaging

Prior to Phase I, several laboratory demonstrations of wide-field magnetic imaging using diamond had been reported [3, 10, 12, 13, 16], but these had not yet shown the sensitivity to DC fields over a wide field of view that would allow for high-fidelity rare cell detection. QDTI worked in collaboration with Ron Walsworth's lab at the Harvard-Smithsonian Center for Astrophysics with a state-of-the-art diamond magnetic imaging apparatus. Several primary performance limitations were identified and solutions were developed to dramatically reduce the effects of each, as described below.

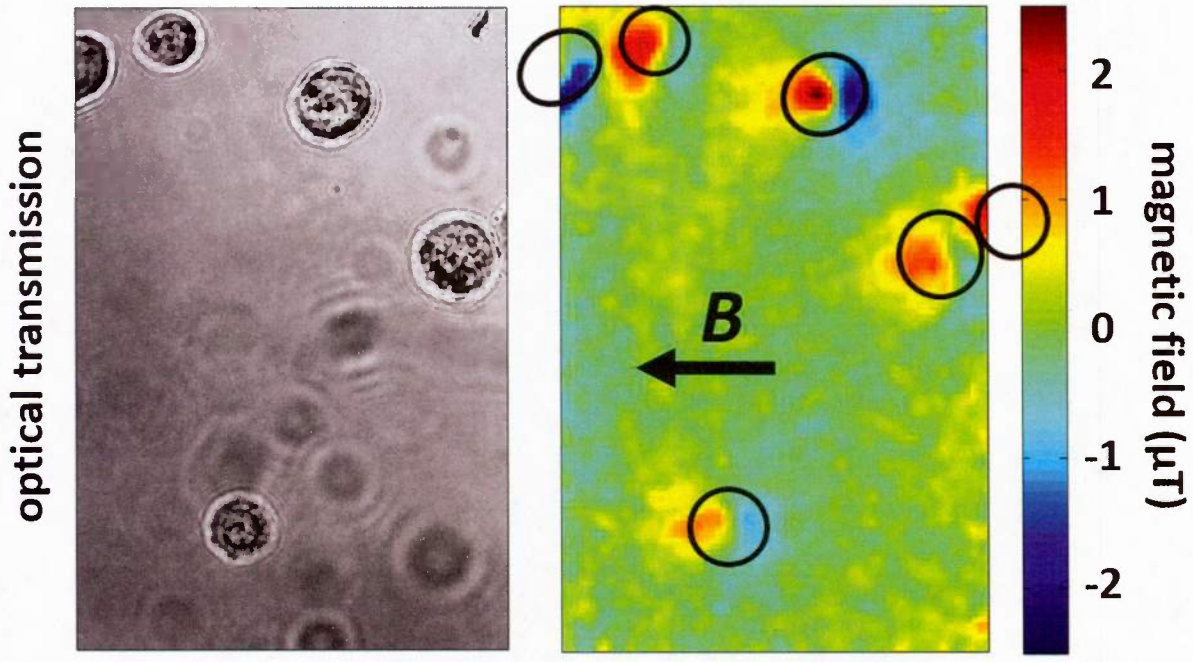

Figure 4: Optical transmission (left) and magnetic (right) images of magnetically-labeled human breast cancer cells (SK-BR-3). Approximate cell locations are outlined as black ellipses in the magnetic image. The magnetic field *B* (direction shown) magnetizes the superparamagnetic MNP tags to produce a dipole field distortion for each cell.

Active tracking of excitation beam intensity fluctuation

Fluctuations in the diamond excitation beam power cause successive images of NV fluorescence to vary in brightness. When the set of images is then analyzed pixel-wise to locate the ESR resonance, this variation is seen as noise on the ESR spectrum. This noise ultimately limits the achievable magnetic field sensitivity. While active stabilization of the excitation power is possible, it is sufficient to simply measure the variation and normalize each image.

An ideal normalization would monitor the intensity profile of the excitation light at the diamond surface. Assuming that the NV fluorescence is linear in excitation intensity (i.e., far from optical saturation), then the NV fluorescence itself provides this information, but only when the microwave field is non-resonant. Hence using the NV fluorescence for normalization requires taking multiple images in rapid succession: both with and without the microwave field. This method can successfully correct for slow variation of the excitation power, but not the fluctuations that are as fast as or faster than the imaging frame speed, typically 10 Hz to 1 kHz.

An alternate method, and the one employed in Phase I, is to monitor the excitation beam power with a beamsplitter and photodiode. Simultaneous use of both arms of the split beam path allows for both imaging and image normalization. While this method is effective for all relevant frequency components of excitation intensity noise, there remain drawbacks. Most importantly, additional noise introduced after the beamsplitter, due for example to vibration of the diamond relative to the excitation beam, is not monitored. Similarly, the two beam paths are unlikely to be matched in polarization sensitivity, implying that fluctuations in excitation beam polarization will introduce new apparent intensity fluctuations after the normalization. With appropriate control of vibration and polarization, however, beam intensity variations were controlled to better than the 10^{-3} level.

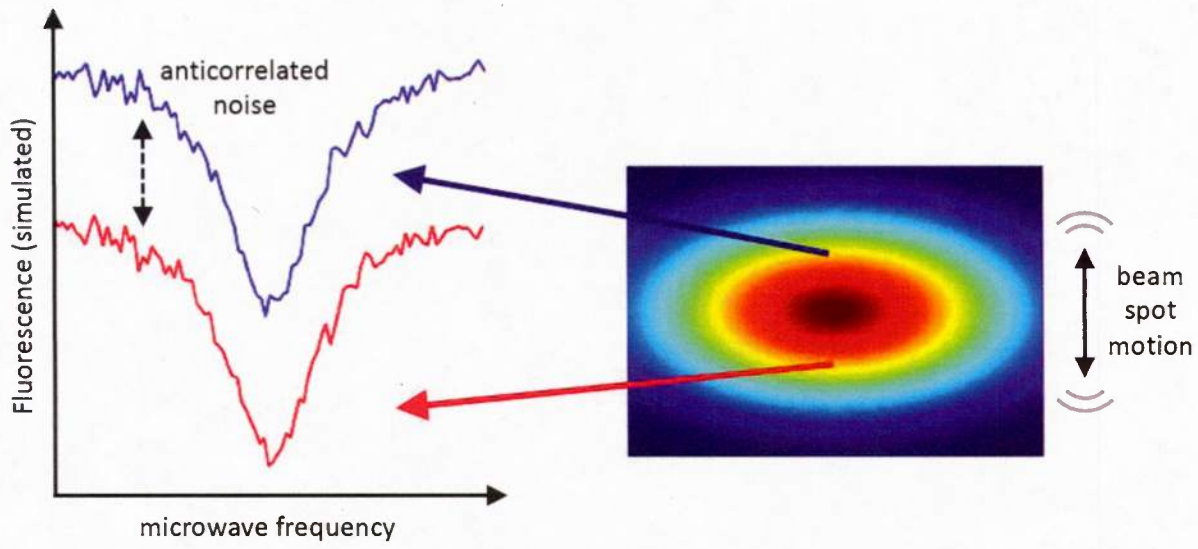

Figure 5: Simulated noise due to beam spot motion. For a non-uniform excitation beam intensity profile (such as the Gaussian spot simulated here), beam motion causes intensity variation at individual pixels. Regions of pixels where the local excitation intensity gradient has opposite sign along the motion axis (origins of blue and red arrows) will experience equal and opposite intensity variation. This variation causes anticorrelated noise between the regions (shown in the simulated ESR spectra at left) which biases the fits in opposite directions. Hence the magnetic fields deduced from the two spectra, in the absence of an actual magnetic field, will be nonzero and opposite, imprinting an intensity gradient pattern artifact onto the magnetic field image.

Minimized excitation beam pointing instability

Even after correcting for excitation beam intensity fluctuations, beam motion with respect to the diamond surface can introduce additional noise. Given a non-uniform beam intensity profile (e.g., the Gaussian profile shown in Figure 5), there are intensity gradients in the fluorescence image that vary in direction and sign. If the intensity profile is translated in the image plane due to beam motion, then pixels in the image will brighten or dim depending on whether the local intensity gradient has a component parallel or antiparallel to the motion, respectively. Since the motion is the same at all pixels, this creates correlated intensity noise among pixels (Figure 5), with the largest noise occurring where the intensity gradients are greatest.

Very slight motion can produce significant noise in this manner. For example, consider a centered Gaussian beam profile that varies by a factor of two over a 30-μm field of view. Beam motion of 1 μm, corresponding to only 1 μrad angular variation over a 1 m beam path, will result in approximately 5% intensity fluctuation at the edge of the imaging field of view, with equal and opposite fluctuations at the two edges. This single-pixel variation is significantly larger than the total excitation beam power fluctuations.

Furthermore, noise from beam motion is worse than global excitation power variation because it does not affect all pixels in the same manner. The spatially-correlated noise due to beam motion corrupts the magnetic field images with artifacts of the excitation intensity profile. To understand this, consider a single large beam excursion for one fluorescence image in an otherwise noiseless set of images at different microwave frequencies used for an ESR measurement. In the single noisy image, regions with oppositely-pointing intensity gradients will be either brighter or dimmer, respectively, due to the beam's

motion. Hence the ESR spectrum at each pixel will have one point at this microwave frequency that is anomalously high or low. Finally, the least-squares fits to these spectra will therefore be biased to higher or lower ESR resonant frequency, and hence magnetic field. This effectively imprints the intensity gradient pattern onto the magnetic image, by adding this bias wherever the gradient is large.

QDTI suppressed beam-motion image artifacts by reducing the magnitude of excitation intensity gradients (i.e., flattening and smoothing the excitation beam profile) and by minimizing beam motion. First, the excitation beam was defocused to produce a broader, smoother spot at the diamond. Second, the excitation laser was coupled via a single mode fiber so that angular fluctuations or variation in the laser's spatial mode would be spatially filtered, producing only global intensity fluctuations that can be normalized.

Finally, it is important to note that motion of the imaging system with respect to the diamond surface will have the same effect as beam motion. Hence this motion was also minimized by rigid mechanical support.

Dual-resonance cancellation of diamond strain effects

QDTI studied the impact of crystal strain on diamond magnetic sensing of DC fields. Strain can be caused by many sources, including grown-in crystal dislocations, surface polishing, temperature gradients, and applied mechanical forces. Strain both longitudinal and transverse to the NV axis produces ESR life shifts that can be misinterpreted as magnetic field [25]. Figure 6(a) shows an example of such line shifts due to dislocation strain in CVD-grown single-crystal diamond. Dislocation strain is especially problematic for magnetic imaging because it generates spatial features spanning 1–100 µm with associated line shifts that can be greater than the Zeeman shift from a 10 µT magnetic field. Without controlling for strain, high-sensitivity DC magnetic imaging at these length scales is therefore not possible.

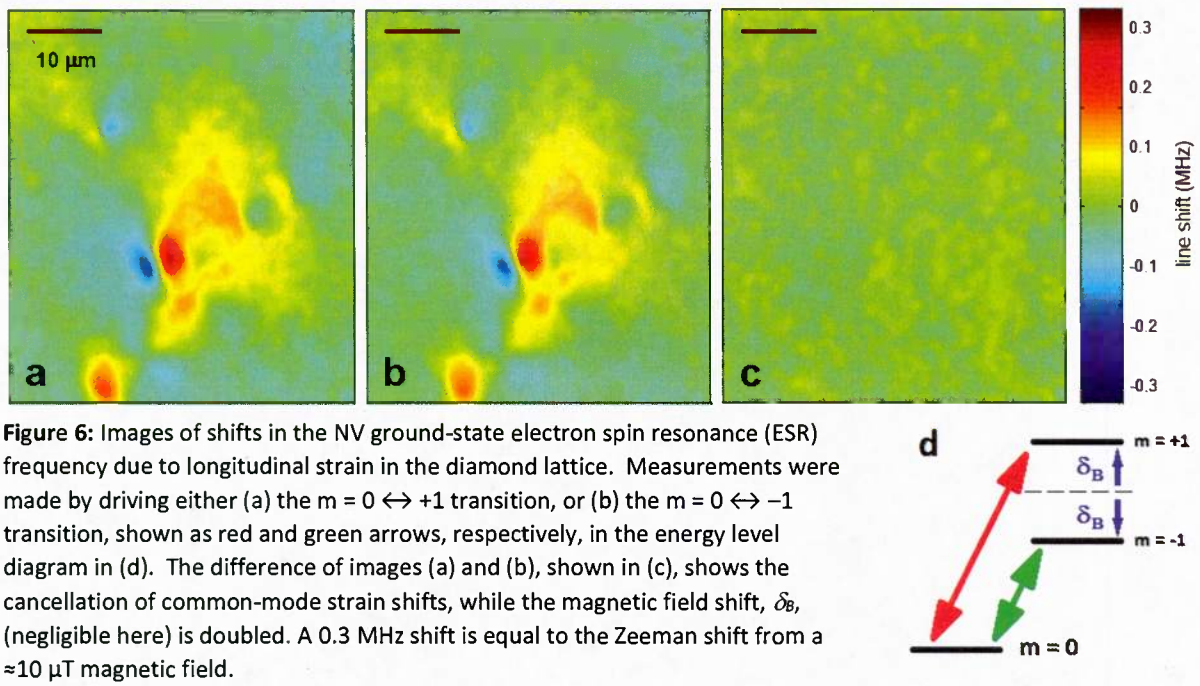

Figure 6: Images of shifts in the NV ground-state electron spin resonance (ESR) frequency due to longitudinal strain in the diamond lattice. Measurements were made by driving either (a) the m = 0 ↔ +1 transition, or (b) the m = 0 ↔ −1 transition, shown as red and green arrows, respectively, in the energy level diagram in (d). The difference of images (a) and (b), shown in (c), shows the cancellation of common-mode strain shifts, while the magnetic field shift, δ_B, (negligible here) is doubled. A 0.3 MHz shift is equal to the Zeeman shift from a ≈10 µT magnetic field.

Fortunately, strain shifts can be mitigated in several ways, including: (1) by employing low-strain diamond material [26] for which any shifts are minimal compared to Zeeman shifts from the sample; (2) subtracting normalization images taken with a clean diamond surface, assuming the strain shifts are static; or (3) employing dual-ESR-resonance cancellation of strain shifts. In the latter method, separate measurements of the $m = 0 \leftrightarrow -1$ and $0 \leftrightarrow +1$ ESR resonances (see level diagram in Figure 6(d)) are subtracted to eliminate common-mode shifts. Since the two resonances experience opposite Zeeman shifts, this difference yields twice the signal from magnetic fields, independent of longitudinal strain. Transverse strain shifts are themselves suppressed by the ratio of the strain shift to the Zeeman shift, and hence can be dramatically reduced with modest bias magnetic field strength of 1–10 mT.

Employing this dual-resonance cancellation method, QDTI demonstrated that signal features related to strain can be removed from ESR-based magnetic field images. For each point in the ESR spectrum, two fluorescence exposures were made in succession at a microwave frequency near to each resonance. Each of the two sets of exposures was analyzed separately to generate two magnetic field images. The difference of these two images shows no visible strain features (Figure 6(c)). Since the two magnetic field images are each an independent measurement, there is no loss of statistical sensitivity compared to taking the same total number of exposures with a single ESR resonance, making this is a highly efficient and effective method.

5. Technical progress: rare cell detection

QDTI's progress in Phase I in improving the technical performance of diamond magnetic imaging allowed for more rapid and sensitive detection of magnetically labeled cells. In tandem with this magnetic imaging development, QDTI also made significant progress in demonstrating the key capabilities for using diamond magnetic imaging for a rare cell detection assay. This progress, detailed below, represents critical first steps toward an ultimate Phase II goal of validating this assay as a clinical diagnostic tool.

Magnetic imaging of cells in liquid

QDTI demonstrated magnetic imaging of cancer cells in a liquid buffer solution, a capability that is important for creating a viable high-throughput assay. Scanning the tens of millions of nucleated cells in a standard patient sample simultaneously in the same field of view is likely improbable, as it would require a diamond sensor area of order 100 cm^2. It is therefore critical that a diamond-based detection platform be capable of analyzing 10–100 fields of view in rapid succession across a single diamond sensor. To facilitate rapid delivery and removal of cells to and from the sensor surface, QDTI intends to use a fluid-based cell migration system.

Larger magnetic signals can generally be obtained by drying the cells on the diamond. The magnetic field varies as r^{-3}, where r is the distance from an individual MNP to the NV centers. Hence collapsing the cell and its MNP tags onto to the diamond surface reduces r and considerably boosts the magnetic signature of the labeled cell. However, drying the cells is slow and not conducive to rapid repetitions of the imaging procedure. Furthermore, an ideal cell counting assay preserves the viability of the cells for later analysis. Particularly in the case of CTCs, the heterogeneity of cancer types and of CTCs within a given patient makes further study important (e.g., genetic identification of the CTCs to determine which chemotherapy treatment will be most effective).

For these reasons, the capability for imaging magnetically tagged cells in liquid is important for successful implementation of the rare cell detection assay. All images of cancer cells presented in this report have been obtained from cells in liquid.

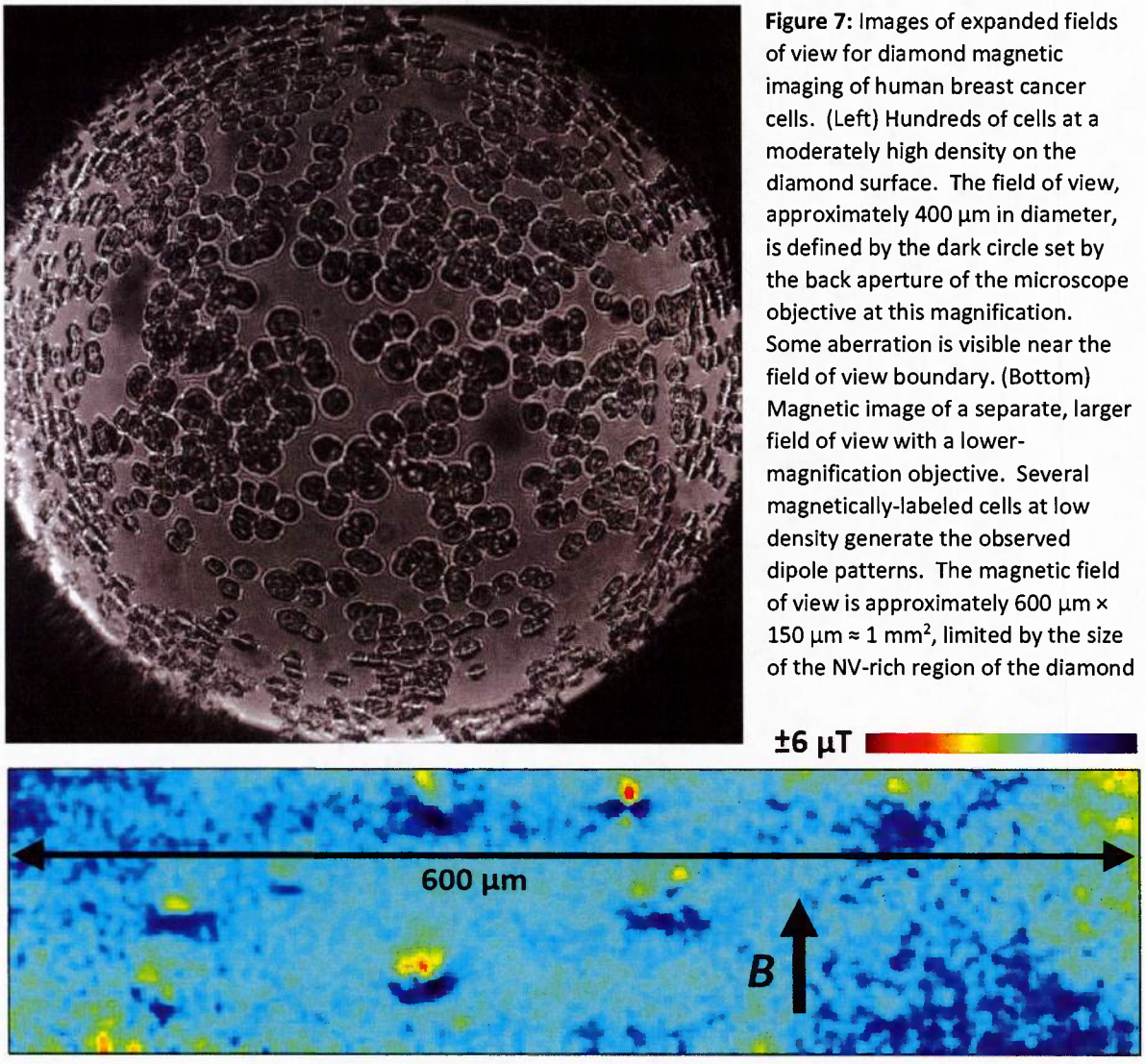

Figure 7: Images of expanded fields of view for diamond magnetic imaging of human breast cancer cells. (Left) Hundreds of cells at a moderately high density on the diamond surface. The field of view, approximately 400 μm in diameter, is defined by the dark circle set by the back aperture of the microscope objective at this magnification. Some aberration is visible near the field of view boundary. (Bottom) Magnetic image of a separate, larger field of view with a lower-magnification objective. Several magnetically-labeled cells at low density generate the observed dipole patterns. The magnetic field of view is approximately 600 μm × 150 μm ≈ 1 mm^2, limited by the size of the NV-rich region of the diamond

Field of view expansion

QDTI expanded the magnetic imaging field of view over the course of Phase I to demonstrate the unique advantage of NV-diamond for highly parallel magnetic sensing. Unlike with other magnetometry technologies, nanoscale NV centers can be packed tightly into an ensemble of independent sensors that can be remotely and simultaneously addressed with spatial resolution well under 1 μm. No sensor electrical contact is needed, replacing complex wiring for SQUID or Hall sensor arrays with a single continuous diamond chip, and no serial scanning of the imaging field is required. Current technologies for single-cell magnetic detection are based on counting cells one by one in series [22], but a diamond sensor has the capacity to dramatically improve detector throughput by scanning in parallel.

As the magnetic imaging field of view grows, more and more cells can be simultaneously interrogated, leading not only to shorter overall assay time, but also to fewer sequential scanning steps required to process tens of millions of cells. Achieving a field of view of >10 mm^2 is achievable with available single-crystal diamond sensors, and could enable imaging of approximately 100,000 cells at once.

In Phase I, QDTI achieved a field of view of ≈0.1 mm^2 (Figure 7), significantly larger than what had been previously demonstrated and limited only by the size of the NV-rich area of the diamond sensor. It is important to note that the imaging resolution need only be that which is sufficient to detect a cell-sized (≈10 μm) magnetic field feature. Hence diffraction-limited microscopy is not necessary. Similarly, a few pixels per cell is sufficient to obtain the binary output from each cell: is it magnetically labeled, or not? The image in Figure 7 clearly has far better resolution than needed, which can be sacrificed in order to accommodate the need for a larger field of view.

Increased signal with more magnetic MNPs

In order to create a strong cellular magnetic signal for reliable detection, QDTI tested several types of superparamagnetic iron oxide MNPs for labeling target cells. As described in Section 3 above, the magnetic moment of a superparamagnetic particle aligns with an applied magnetic field faster than the measurement time. This allows for an ensemble of N particles to produce a large additive magnetic field, in contrast to the $\approx N^{1/2}$ times smaller field that would result from the same number of ferromagnetic particles whose magnetic moments have random fixed orientations. This additive effect is useful for achieving high specificity and sensitivity detection: using the cumulative effect of tens or hundreds of thousands of superparamagnetic MNPs enables cells to be strongly labeled, while individual unbound MNPs remain too weak to be observed [22].

In Phase I, QDTI labeled cells with three different MNP types: (1) 7-nm diameter core Fe_2O_3 (maghemite); (2) 15-nm core Fe_3O_4 (magnetite); and (3) 20-nm core Fe_3O_4. In each case, "core" refers to the iron oxide at the center of the particles, which are then coated with one or more materials for stability, biocompatibility, and surface functionalization. Initial feasibility studies with macrophage cells used the 7-nm core particles (cross-linked iron oxide (CLIO) dextran-coated particles developed at MGH). The particles with larger core diameters (obtained from Ocean NanoTech, LLC) were used for later work in order to increase the magnetic signal. Larger particles with more iron oxide yield larger cellular fields, given a fixed number of attachment sites on the cell surface. Larger fields, in turn, allow for more rapid magnetic imaging, with the imaging time dropping by the square of the increase in field (for unchanged SNR).

Superparamagnetism does not persist indefinitely, however, as the particle size is increased. The energy needed for the particle magnetic moment to change direction with respect to the crystal axes (called the anisotropy energy) grows in proportion to the particle volume. When this energy is much larger than available thermal energy, the magnetic moment is "blocked," and can no longer follow changes in the magnetic field (although it may still be possible for the particle to align by rotation in solution). Furthermore, more strongly magnetic particles can bind together due to the magnetic dipole-dipole interaction, forming clumps that are detrimental to cell labeling and detection. Hence there exists an optimal particle size for a given application.

From comparative testing, QDTI determined that the magnetic signal obtained using 20-nm vs. 15-nm core particles was indeed greater by a factor of approximately $(20/15)^3 \approx 2.37$. Therefore no detrimental size effect is yet apparent with 20-nm iron oxide particles. It is thus likely that the particle size can be further increased to magnify the magnetic labeling. In addition, other particle parameters, such as chemical composition and surface coating, further affect the strength and robustness of MNP labeling. QDTI only began to explore this parameter space in Phase I. QDTI expects that significant increases in cellular magnetic field are possible using currently available MNPs, and further improvements can likely be made with focused optimization of novel MNPs.

Demonstration of labeled cancer cells detected amid background of unlabeled cells

Bringing together all of the technical progress described above, QDTI performed a proof-of-principle demonstration of diamond magnetic imaging used for rare cell detection. First, a sample of magnetically-labeled human breast cancer cells was prepared using the procedure outlined in Section 4. This sample was then mixed with a sample of unlabeled cells of otherwise identical preparation, with the resulting mixture containing approximately 10% labeled cells and 90% unlabeled cells. Cells from this mixture were placed on the diamond surface and imaged both optically and magnetically (Figure 8).

A simple image processing procedure allows for identification of the magnetically labeled cells by recognizing a characteristic magnetic field pattern. Assuming that the labeled cell can be modeled as a spherical shell of magnetized material, then the resulting magnetic field is that of a single dipole at the cell's center. To approximate this field, a filter function was constructed as the product of a Gaussian function in the vertical direction and the derivative of a Gaussian in the horizontal direction (Figure 8(b) inset). This filter function was then convolved with the raw magnetic image. The visible dipole structures in the magnetic image show up as bright peaks in the convolution in places where the magnetic field reasonably matches the filter function.

The convolution image is then subjected to a threshold which selects magnetic dipole fields having the form of the filter function and a magnitude greater than ±1 μT. The four regions of the image above this threshold are overlaid in red on the optical transmission image (Figure 8(c)) and are seen to correspond to five distinct cells (the two cells on the far right side of the image are in contact, with overlapping dipole fields, and so show up as one above-threshold region). The five positive detections observed out of 70–80 total cells in the image is within one standard deviation of the expected number (given a 10% minority fraction of labeled cells). While no independent identification was made of the labeled cells (e.g., with additional fluorescent labeling), this result is consistent with 100% detection sensitivity and suggests that labeled cells can be faithfully identified by diamond magnetic imaging.

QDTI also demonstrated that the magnetic imaging can be done rapidly. Figure 9 shows the same field of view shown in Figure 8, imaged in less than one minute, which yields the same detection result. QDTI is therefore confident that rapid imaging of many cells in parallel is feasible, especially considering that there is considerable room for targeted improvement of the Phase I imaging apparatus.

6. Summary and future outlook

In this Phase I period, QDTI fulfilled its objectives for bringing diamond magnetic imaging closer to commercial implementation. First, an achievable, high-value target application was identified: detection of magnetically-labeled rare cells, and of CTCs in particular. There is clear clinical utility in counting CTCs in patient blood samples, in terms of both disease progression and treatment monitoring. Furthermore, this need is not well addressed by existing technologies, which are too insensitive, too slow, and too expensive. A rare cell detector based on imaging target cells in parallel with a diamond sensor has the capacity to excel on all these fronts.

Second, significant technical progress was made in a short period of time to advance the capabilities of diamond magnetic imaging. Several primary sources of noise or technical artifacts were identified and suppressed to enable faster and more sensitive images. This progress serves to advance the technology generally and helps to enable many different application directions. For example, the demonstration of cancelling strain shifts over the wide imaging field is applicable to magnetic imaging of any sample for which sensitivity better than 10 μT is desired.

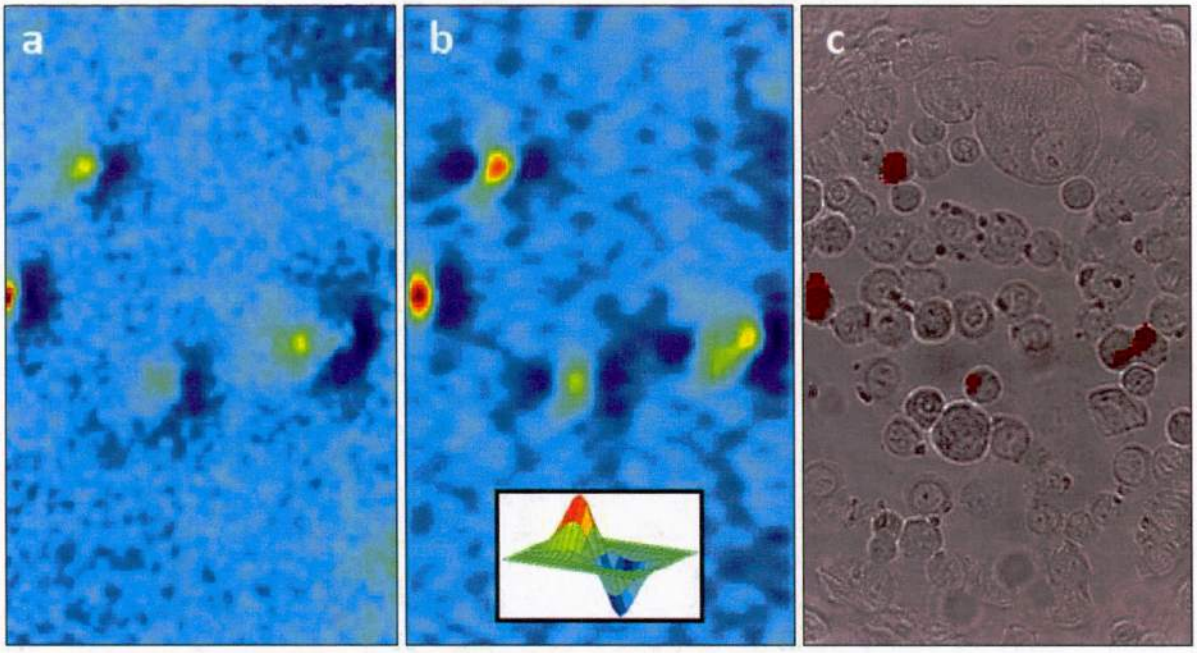

Figure 8: (a) Magnetic field patterns produced by five magnetically-labeled human SK-BR-3 cancer cells laying on the surface of the diamond sensor (color scale is ±2 μT). The two cells on the far right of the image are in contact and produce overlapping magnetic fields. (b) The magnetic field image after spatial filtering with the dipole filter shown in the inset, which converts similar structures to peaks. (c) Overlay of optical transmission image corresponding to the same field of view as (a) and (b), along with regions within peaks from (b) corresponding to dipoles above ±1 μT. Note that many unlabeled cells are also present in the field of view with no detectable fields.

Figure 9: Same imaging field of view and conditions as in Figure 8, except with imaging time cut by a factor of five, to less than one minute. While the noise of the magnetic image is increased, the same five cells are well distinguished from background

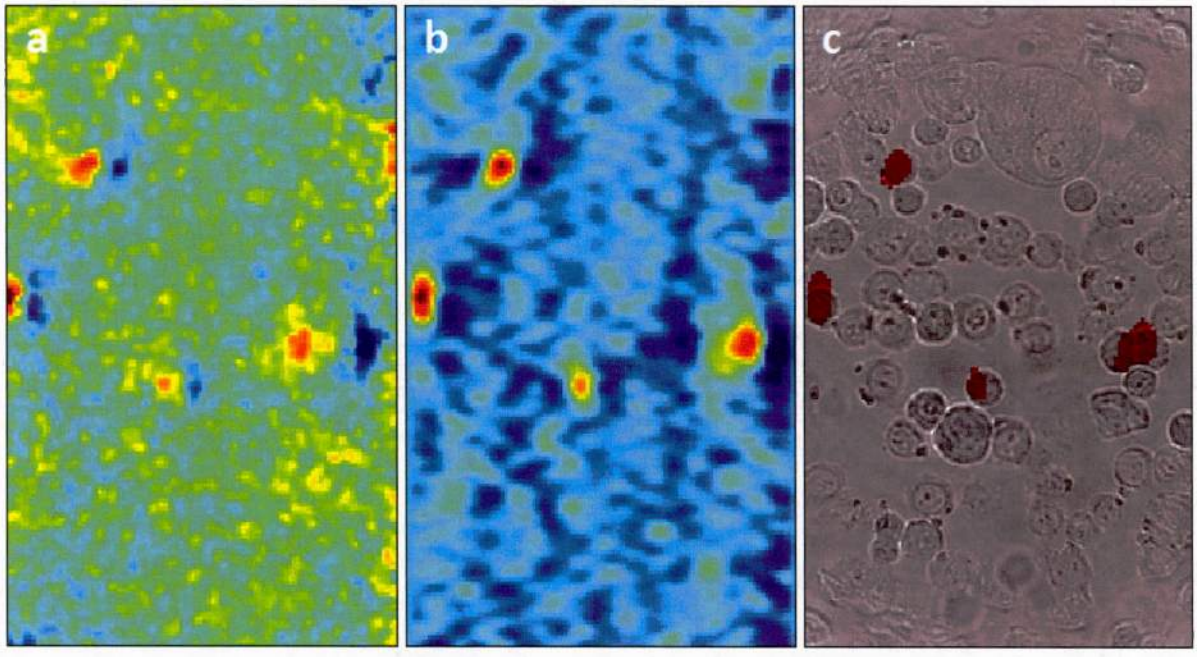

Finally, the feasibility of rare cell detection with diamond was demonstrated. Magnetically-labeled human breast cancer cells were detected amid a background of unlabeled and otherwise undifferentiated candidates. Detection SNR was sufficient for highly sensitive cell counting, and reliable imaging in less than one minute was demonstrated. This Phase I effort has revealed the potential for diamond magnetic imaging to be a powerful clinical tool. The combination of high-fidelity magnetic imaging with rapid, parallel wide-field detection can revolutionize detection of rare biological targets, including not only CTCs but also pathogens and stem cells.

7. References

1. *High-sensitivity diamand magnetameter with nonascale resalutian*. J.M. Taylar, P. Cappellara, L. Childress, L. Jiang, D. Budker, P.R. Hemmer, A. Yacoby, R. Walsworth, and M.D. Lukin, Nature Physics **4**, 810 (2008).
2. *Nonoscole mognetic sensing with on individuol electronic spin in diomond*. J.R. Maze, P.L. Stanwix, J.S. Hodges, S. Hong, J.M. Taylor, P. Cappellaro, L. Jiang, A.S. Zibrov, A. Yacoby, R. Walsworth, and M.D. Lukin, Nature **455**, 644 (2008).
3. *Magnetic field imaging with NV ensembles*. L.M. Pham, D. Le Sage, P.L. Stanwix, T.K. Yeung, D. Glenn, A. Trifanav, P. Cappellara, P.R. Hemmer, M.D. Lukin, H. Park, A. Yacaby, and R.L. Walswarth, New Jaurnal af Physics **13**, 045021 (2011).
4. *Quontum cantral af praximal spins using nanascale magnetic resanance imaging*. M.S. Grinalds, P. Maletinsky, S. Hang, M.D. Lukin, R.L Walsworth, and A. Yacoby, Nature Physics **7**, 687 (2011).
5. *A rabust scanning diamand sensar far nonascole imoging with single nitragen-voconcy centres*. P. Maletinsky, S. Hang, M.S. Grinalds, B. Hausmann, M.D. Lukin, R.L. Walswarth, M. Lancar, and A. Yacaby, Nature Nanotechnology **7**, 320 (2012).
6. *Efficient photon detection from color centers in o diomond opticol woveguide*. D. Le Sage, L.M. Pham, N. Bar-Gill, C. Belthangady, M.D. Lukin, A. Yacaby, and R.L. Walswarth. Physical Review B 85, 121202(R) (2012).
7. *Enhanced salid-stote multi-spin metralagy using dynomicol decaupling*. L. M. Pham, N. Bar-Gill, C. Belthangady, D. Le Sage, P. Cappellara, M. D. Lukin, A. Yacaby, and R. L. Walswarth. Physical Review B, 86, 045214 (2012).
8. *Nonoscole mognetometry with NV centers in diomand*. S. Hang, M. S. Grinalds, L. M. Pham, D. Le Sage, L. Luan, R. L. Walswarth, A. Yacaby. Materials Research Saciety Bulletin 38, 155 (2013).
9. *Nonoscole mognetic imoging of o single electron spin under ombient canditions*. M. S. Grinalds, S. Hong, P. Maletinsky, L. Luan, M. D. Lukin, R. L. Walswarth, A. Yacoby. Nature Physics **9**, 215 (2013).
10. *Opticol mognetic imoging of living cells*. D. Le Sage, K. Arai, D. R. Glenn, S. J. DeVience, L. M. Pham, L. Rahn-Lee, M. D. Lukin, A. Yacaby, A. Kameili, and R. L. Walswarth. Nature **496**, 486-489 (2013).
11. *Nonascale imaging magnetametry with diamand spins under ombient conditions*. G. Balasubramanian, I. Y. Chan, R. Kolesov, M. Al-Hmoud, J. Tisler, C. Shin, C. Kim, A. Wajcik, P. R. Hemmer, A. Krueger, T. Hanke, A. Leitenstorfer, R. Bratschitsch, F. Jelezko, and J. Wrachtrup, Nature Letters **455**, 648 (2008).
12. *Vector mognetic field microscopy using nitrogen voconcy centers in diomond*. B. J. Maertz, A. P. Wijnheijmer, G. D. Fuchs, M. E. Nawakawski, and D. D. Awschalom, Applied Physics Letters **96**, 092504 (2010).
13. *High sensitivity magnetic imaging using an array af spins in diomond*. S. Steinert, F. Dolde, P. Neumann, A. Aird, B. Naydenov, G. Balasubramanian, F. Jelezko, and J. Wrachtrup, Review of Scientific Instruments **81**, 043705 (2010).
14. *Nonoscole nucleor mognetic resononce with o nitrogen-voconcy spin sensor*. H. J. Mamin, M. Kim, M. H. Sherwood, C. T. Rettner, K. Ohna, D. D. Awschalom, and D. Rugar, Science **339**, 557 (2013).
15. *Nucleor mognetic resononce spectroscopy an o (5-nanameter)^3 sample volume*. T. Staudacher, F. Shi, S. Pezzagna, J. Meijer, J. Du, C. A. Meriles, F. Reinhard, and J. Wrachtrup, Science **339**, 561 (2013).
16. *Magnetic spin imaging under ombient canditians with sub-cellular resalutian*. S. Steinert, F. Ziem, L. T. Hall, A. Zappe, M. Schweikert, N. Götz, A. Aird, G. Balasubramanian, L. Hollenberg, and J. Wrachtrup, Nature Communications **4**, 1607 (2013).

17. *Suppression of spin-both dynomics for improved coherence of multi-spin-qubit systems*. N. Bar-Gill, L.M. Pham, C. Belthangady, D. Le Sage, P. Cappellaro, J.R. Maze, M.D. Lukin, A. Yacoby, and R.L. Walsworth, Nature Communications **3**, 858 (2012).
18. *Concer Focts ond Figures 2013*. American Cancer Society. Atlanta: American Cancer Society (2013).
19. *Deoths: Preliminory Doto for 2011*. Centers for Disease Control and Prevention. National Vital Statistics Reports **61**(6) (2012).
20. *Circuloting Tumor Cells Predict Survivol Benefit from Treotment in Metostotic Costrotion-Resistont Prostote Concer*. J. S. de Bono, H. I. Scher, R. B. Montgomery, C. Parker, M. C. Miller, H. Tissing, G. V. Doyle, L. W. W. M. Terstappen, K. J. Pienta, and D. Raghavan. Clinical Cancer Research **14**, 6302-6309 (2008).
21. *Cose Study: 57-yeor-old mole potient with mCRC with liver metostoses*. Stephan Cohen, MD, Associate Medical Director, Fox Chase Cancer Partners, Philadelphia, PA.
22. *Ultrosensitive Clinicol Enumerotion of Rore Cells ex Vivo Using o Micro-Holl Detector*. D. Issadore, J. Chung, H. Shao, M. Liong, A. A. Ghazani, C. M. Castro, R. Weissleder, H. Lee. Science Translational Medicine **4** 141ra92 (2012).
23. *Mognetic Iron Oxide Nonoporticles: Synthesis, Stobilizotion, Vectorizotion, Physicochemicol Chorocterizotions, ond Biologicol Applicotions*. S. Laurent, D. Forge, M. Port, A. Roch, C. Robic, L. V. Elst, R. N. Muller. Chemical Reviews **10**8, 2064-2110 (2008).
24. *Mocrophoge endocytosis of superporomognetic iron oxide nonoporticles*. I. Raynal, P. Prigent, S. Peyramaure, A. Najid, C. Rebuzzi, and C. Corot, Investigative Radiology **39**, 56 (2004).
25. *Electric-field sensing using single diomond spins*. F. Dolde, H. Fedder, M. W. Doherty, T. Nöbauer, F. Rempp, G. Balasubramanian, T. Wolf, F. Reinhard, L. C. L. Hollenberg, F. Jelezko, and J. Wrachtrup, Nature Physics **7**, 459 (2011).
26. *Control of surfoce ond bulk crystolline quolity in single crystol diomond grown by chemicol vopour deposition*. I. Friel, S. L. Clewes, H. K. Dhillon, N. Perkins, D. J. Twitchen, and G. A. Scarsbrook, Diamond & Related Materials **1**8, 808 (2009).

8. Publications this period

There were no publications sponsored by this contract in this reporting period.